IEEE Access
Multidisciplinary | Rapid Review | Open Access Journal

Received February 18, 2021, accepted March 9, 2021, date of publication March 12, 2021, date of current version March 22, 2021.

Digital Object Identifier 10.1109/ACCESS.2021.3065666

Lower Limb Model Based Inertial Indoor Pedestrian Navigation System for Walking and Running

WANLING LI, ZHI XIONG, YIMING DING, ZHIGUO CAO, AND ZHENGCHUN WANG

College of Automation Engineering, Nanjing University of Aeronautics and Astronautics, Nanjing 210000, China

Corresponding author: Zhi Xiong (xiongzhi@nuaa.edu.cn)

This work was supported in part by the projects in the Special Zones for National Defense Science and Technology Innovation, and in part by the Natural Science Foundation of China under Grant 61873125 and Grant 62073163, and in part by the Fundamental Research Funds for the Central Universities under Grant NZ2020004.

ABSTRACT Foot-mounted inertial navigation systems are suitable in GNSS denied environment for special tasks such as fire rescue, soldier, etc. These tasks are often accompanied by vigorous movements such as running and jumping, which is a challenge for the Zero Velocity Update (ZUPT) based inertial navigation system. As the speed increases, the inertial sensor drift increases, while the zero-velocity interval shortens, making the gait detection more difficult and resulting in a limited error correction. And as the motion intensifies, the stability of the system decreases. A multi-node inertial pedestrian navigation system based on the lower limb model constraint is proposed in this paper. Our first contribution in this paper is studying a simplified adaptive zero-bias estimation algorithm. The changes in velocity and angular velocity between two steps are used to estimate and compensate for the drift of accelerometers and gyroscopes. Our second contribution is proposing a novel gait segmentation method by lower limb motion statistics feature. A hybrid detection model of dual IMU is conducted to improve the accuracy of gait recognition. After that, the maximum distance inequality constraint is studied to correct the position error when the still phase is not available in vigorous movement. The final contribution is studying the chi-square fault detection method to improve the stability of KF. Multiple experiments prove that the proposed multi-node inertial pedestrian navigation system is effective in dealing with various challenging in walking, running, and hybrid motion pedestrian inertial navigation problems which could achieve less than 0.3% average distance error.

INDEX TERMS Multi-node constraint, motion characteristic statistics, adaptive zero-bias estimation, fault detection.

I. INTRODUCTION

In recent years, the demand for indoor positioning in special tasks such as firefighting, the underground prospecting, and the location-based service is increasing gradually. At present, the major indoor positioning methods include positioning technology based on external sources, such as WiFi, Bluetooth, Ultra Wide Band (UWB), and passive navigation, such as inertial navigation [1]. The inertial navigation system based on Miniature Inertial Measurement Unit(MIMU) has the advantages of autonomy, low cost, and wearable, which can meet the navigation requirements under a special environment.

The associate editor coordinating the review of this manuscript and approving it for publication was Kegen Yu.

However, the low precision and high noise of the MIMU result in accumulating positioning errors [2]. To compensate for gyroscopes and accelerometers errors, researchers have proposed error modeling methods such as auto regressive(AR), moving average(MA) and auto regressive moving average(ARMA) [3]–[6]. These methods require a prior identification model. However, MIMU is easily affected by the environment, while the complex environment of special tasks and the violent movement of operators will lead to time-varying errors, so it is difficult to describe with a definitive mathematical model.

The biomechanical models constraint is an effective mean to suppress the error of the navigation system. There is cyclic movement of the foot [7]. In the whole phases of a stride, the bottom of the sole in contact with the ground for

a short period called the still phase, others are called the swing phase. In a foot-mounted inertial pedestrian navigation system, the Zero Velocity Update(ZUPT) aided algorithm is the most effective error correction method [8], and the key to this algorithm is zero-velocity detection. The traditional method of zero-velocity detection using a fixed threshold [9], [10], which cannot adapt to different persons at different speeds. Therefore, some scholars have proposed adaptive zero-velocity detection methods, such as motion state classification based on support vector machines [11], Bayesian estimation-based zero-velocity detection methods [12], and LSTM-Based Zero-Velocity Detection [13]. These methods can improve the detection accuracy of still phase, but they require large amounts of data for model training.

Moreover, not all the position error can be estimated and corrected by ZUPT. As the motion speed increases, the length of the zero-velocity range is shortened or even missing causing the ZUPT to fail. So the combination of multi-IMU based on biomechanical models constraint has been explored to improve the accuracy of positioning [14], [15]. In [16], a pedestrian navigation algorithm based on the bipedal distance constraint is proposed, the positioning error reached 1% in a short distance. In [17], the relative distance constrained algorithm and the adaptive co-localization algorithm are proposed, which improved the positioning accuracy by 60% compared to the traditional method. In [18], [19], a bipedal ellipsoidal constraint method is proposed to achieve a three-dimensional bipedal distance constraint, which effectively reduced the heading drift. A bipedal inertial/magnetometer pedestrian positioning method based on adaptive inequality-constrained Kalman filtering is presented in [20], which allows for long-time walking navigation. These methods are effective when walking at slow speed. However, there are two problems remain in multi-IMU navigation systems: the adaptation of the algorithm under vigorous motion, and the initial alignment of multi-IMU.

Multi-IMU data fusion is often achieved by KF, but the KF requires a precise model, however, the probability of false observations increases as the speed of movement increases. So obviously, it is essential to detect and locate the fault within a short time after the occurrence. The chi-square test method is popular for fault detection in navigation field [21], [22]. This approach behaves well in detecting large step faults. However, it is rarely used in pedestrian navigation systems.

In reality, special tasks are often accompanied by vigorous movements such as running and jumping, which is a challenge for the traditional inertial navigation system. Therefore, in the context of indoor positioning under special operations, this paper studies an inertial pedestrian navigation method based on human four-node constraints. The main contributions of this paper are as follows.

(1) Firstly, simplified error estimation and compensation methods are designed for the MIMUs' drift in complex environments. The changes in velocity and angular velocity between two steps are used to estimate and compensate for the drift of accelerometer and gyroscope.

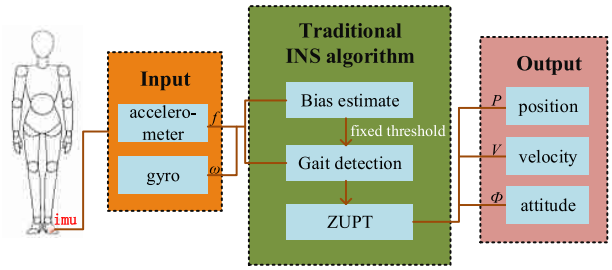

FIGURE 1. Traditional foot-mounted pedestrian navigation system.

(2) Secondly, for the problem of low zero-velocity detection rate during vigorous motion, a hybrid foot and leg detection model is constructed. And then, the bipedal maximum distance inequality constraint is constructed to suppress the heading drift for the missing zero-velocity points.

(3) Finally, we detect the fault of the observation model in KF to confirm the reliability of the system. The semi-physical experiments show that the proposed method can improve the positioning accuracy and robustness of the system.

This paper is organized as follows. In Section 2, presented the improved pedestrian navigation and positioning algorithm, which includes the methods comparison, the adaptive accelerometer and gyroscope zero bias estimation, the adaptive zero-velocity detection, the bipedal inequality constraint algorithm and the fault detection method. In Section 3, experimental results are presented, considering different scenarios and motion modes. Finally, in Section 4 conclusions are drawn.

II. PEDESTRIAN NAVIGATION AND POSITIONING ALGORITHM

A. OVERVIEW

As shown in Figure 1, the traditional foot-mounted navigation system consists of three parts: the zero bias estimation of inertial sensors, the zero-velocity detection, and the ZUPT.

In Fig. 1, f is the acceleration, w is the angular velocity, P, V, Φ are the position, velocity, and attitude, respectively.

The traditional foot-mounted navigation system uses a fixed threshold for zero-velocity detection, which leads to a greater probability of missing detection and misdetection when the motion speed increasing. At the same time, the ZUPT can only correct the position and speed errors but has no observational effect on the heading, so the position error may divergent in vigorous motion.

In order to overcome the shortcomings of the traditional foot-mounted navigation system, this paper studies the human lower limb multi-node constrained inertial pedestrian navigation method, and constructs a four-node constrained model, the system model is shown in the figure 2. There are four IMUs, two of which are worn on the feet, others are on the thighs.

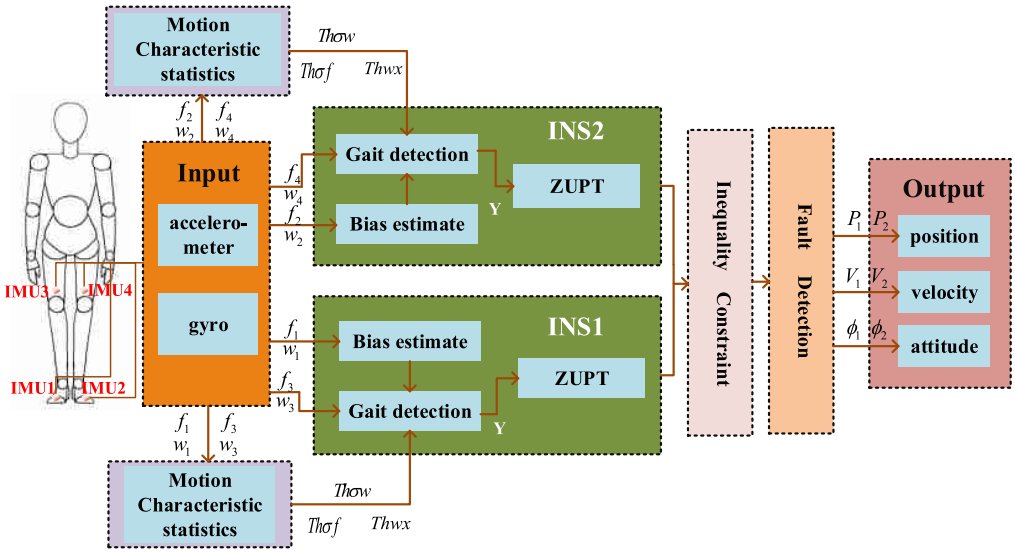

FIGURE 2. Four-node constrained sensor configuration for the human body and pedestrian navigation system diagram.

In Fig. 2, $f_1, f_2, f_3, f_4, w_1, w_2, w_3, w_4$ are the acceleration and angular velocity outputs of IMU1, IMU2, IMU3, and IMU4, respectively. $Th\sigma f$, $Th\sigma w$, $Thwx$ are the acceleration standard deviation threshold, the angular velocity standard deviation threshold, and the x-axis angular velocity threshold, respectively. $P_1, V_1, \Phi_1, P_2, V_2, \Phi_2$ are the position, velocity, and attitude of INS1 and INS2 respectively.

The system contains four IMUs, of which the IMUs strapped to the feet are two navigation subsystems, and the IMUs strapped to the legs are used to aid the subsystems. Zero-velocity is detect by the mixed feature values of the foot and leg. The bipedal inequality constraint takes effect when the bipedal distance is greater than the person's maximum step length. This method can be applied to the motion modes under walking, running, and walking-running.

The following sections will present four parts: adaptive accelerometer and gyroscope zero bias estimation, dual IMU gait detection method, bipedal system heading initial alignment and error correction, and fault detection by dynamic Kalman Filter.

B. ADAPTIVE ACCELEROMETER AND GYROSCOPE ZERO-BIAS ESTIMATION METHODS

Common error modeling and compensation method for MIMU is higher order AR modeling method [23]. This method takes the zero bias of accelerometer and gyro as the state and uses the KF for error estimation, which not only increases the filter computation, but also cause the filter to be unstable or even divergent. In this paper, an adaptive zero bias estimation method for accelerometers and gyroscopes is proposed with zero velocity and zero horizontal attitude angle as constraints in the still phase.

Theoretically, when a person moves, the roll, pitch, and velocity are constant at two adjacent still phases, as shown in equation (1).

$$\left.\begin{aligned} \Delta V &= V_k - V_{k-1} = 0 \\ \Delta\theta &= \theta_k - \theta_{k-1} = 0 \\ \Delta\gamma &= \gamma_k - \gamma_{k-1} = 0 \end{aligned}\right\} \tag{1}$$

where $k-1$ represents the final zero-velocity point in the last still phase, k represents the first zero-velocity point in the current still phase. $\Delta\theta$, $\Delta\gamma$ and ΔV are the pitch, roll and three-axis velocity change from $k-1$ to k, respectively.

The existence of zero bias in the accelerometer and gyroscope leads to unequal velocity and horizontal attitude in two adjacent still phases. Since the zero bias of inertial devices has the greatest impact on the positioning accuracy, and the interval between two adjacent still phase is short under fast movement, the random error is ignored and the inertial device error is assumed to vary uniformly [24]. Then the relationship between the drift error of the accelerometer and gyroscope with the velocity and attitude angle is as follows.

$$\left.\begin{aligned} \nabla_a^b &= \Delta V/T \\ \dot{\theta} &= \Delta\theta/T \\ \dot{\gamma} &= \Delta\gamma/T \end{aligned}\right\} \tag{2}$$

$$\begin{bmatrix} \varepsilon_{nbx}^b \\ \varepsilon_{nby}^b \end{bmatrix} = \begin{bmatrix} \cos\gamma & 0 & \sin\gamma\cos\theta \\ 0 & 1 & -\sin\theta \end{bmatrix} \begin{bmatrix} \dot{\theta} \\ \dot{\gamma} \\ \dot{\psi} \end{bmatrix} \tag{3}$$

where $T = t_k - t_{k-1}$ is the time interval between the end of the last still phase and the beginning of the current still phase, ε_{nbx}^b and ε_{nby}^b are the drift error of the x-axis and y-axis gyroscope, ∇_a^b is the drift error of accelerometer, $\dot{\psi}$ is the change of heading angle. In equation (3), since the rotation invariance of the rigid body, there is a conversion relationship between the angular rate and the attitude angular velocity, a coordinate system conversion is required.

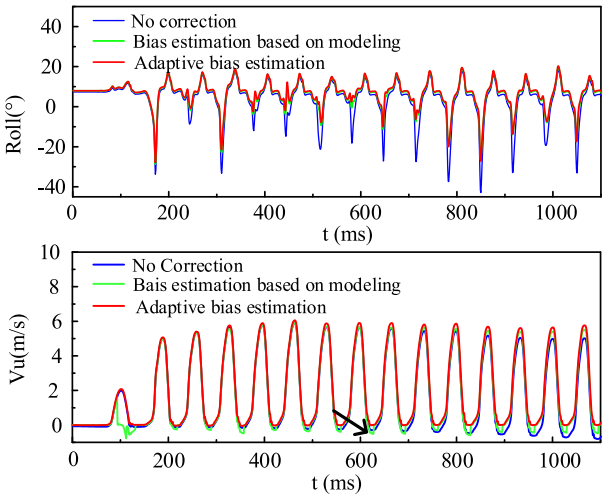

FIGURE 3. Comparison of the effects of different zero bias estimates.

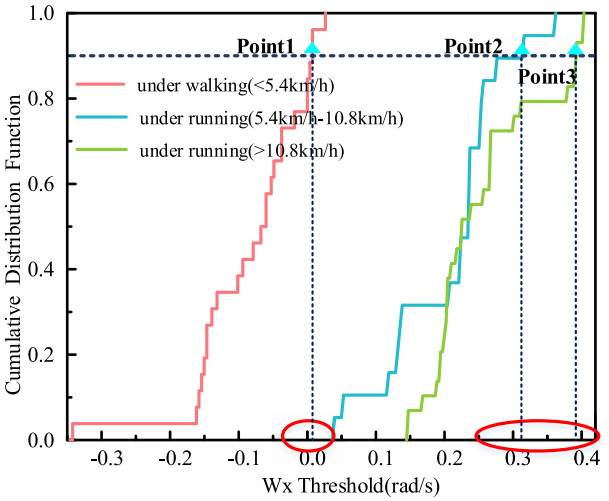

FIGURE 4. PDF curve of X-axis angular velocity at different velocities.

While in the swing state, the accelerometer and gyroscope drift errors are removed in real-time, as shown in equation (4).

$$\left.\begin{aligned} w_{tx} &= w_{tx} - \varepsilon^b_{nbx} \\ w_{ty} &= w_{ty} - \varepsilon^b_{nby} \\ a_t &= a_t - \nabla^b_a \end{aligned}\right\} \tag{4}$$

where w_{tx} and w_{ty} are the angular rate of gyroscope, a_t is the acceleration of the accelerometer.

Using the same set of sensor data of running motion, comparing the roll angle and the up velocity obtained under no corrections, estimated based on AR model, and the adaptive accelerometer and gyroscope zero-bias estimation methods in this paper, the results are shown in Fig. 3. As shown in the figure, the velocity drifts with time in the no correction. The AR can reduce the velocity drift to a certain extent, but it can only correct in the still phase. As shown by the arrows in the figure, there is a sudden change of velocity in the still phase. The main reason is that errors are only corrected when measured is available. In contrast, the adaptive zero-bias estimation method proposed in this paper can effectively suppress the attitude and velocity drifts. Moreover, The CA modeling method is done by KF for error estimation, while this method has a simple model, which can simplify the computation process, save the computation time.

C. DUAL IMU GAIT DETECTION METHOD BASED ON STATISTICAL ESTIMATION OF MOTION CHARACTERISTICS

At present, the detection methods based on fixed thresholds of the single foot are suited for normal walking pace [25], [26]. However, when the speed becomes higher, the threshold needs to be updated, since the duration of the still-phase cannot be detected by the same threshold.

To solve the problem, this paper constructs a hybrid detection model of dual IMU for leg and foot, uses the Euclidean distance of acceleration and angular velocity for motion mode identification, and uses the statistically estimated values under dynamic motion as the still phase's thresholds. The detection process is divided into three main steps as follows.

Step 1, data pre-processing. Collect the IMU data under walking and running movement, then obtain the still phase threshold for each state by frequency statistics. The method is as follows. We take the maximum probability density of the sensor output as the still phase threshold.

$$Th\sigma_f = argmax(P(\sigma_{f_i}))+\delta_f \quad i \in (1, 500) \tag{5}$$

$$Th\sigma_w = argmax(P(\sigma_{w_i}))+\delta_w \quad i \in (1, 500) \tag{6}$$

$$Thw_x = argmax(P(w_{x_i}))+\delta_{w_x} \quad i \in (1, 500) \tag{7}$$

where i is the sample point, σ_f and σ_w represent the standard deviation of acceleration and the standard deviation of angular velocity. δ_f, δ_w and δ_{w_x} are the Maximum permissible error, w_x is the x-axis angular velocity. $Th\sigma_f$, $Th\sigma_w$ and Thw_x are the thresholds, respectively.

Since the IMU data are highly aggregated in the still phase, the probability of the data occurring in the still phase will be greatest when the data are counted at an interval. We selected 500 IMU data for frequency statistical analysis. As shown in Fig. 5, the fig(a) and fig(b) show the X-axis angular velocity curve and X-axis angular velocity probability density curve, fig(c) and fig(d) show the acceleration standard deviation curve and its probability density curve, fig(e) and fig(f) show the angular velocity standard deviation curve and its probability density curve. The blue line in the figure is the IMUs' data, the histogram is the probability density distribution of the IMUs' data, and the red line is the value at the maximum probability. The blue circles in the figure come out with the value at maximum probability density. It can be seen that the highest frequency and highest probability density occur at the moment of the still phase.

We asked one tester walks (less than 5.4km/h), jogs (5.4km/h-10.8km/h) and runs fast (>10.8km/h), the X-axis angular velocity threshold probability density function(PDF) obtained by the method in Step 1 is shown in Fig. 4. The red, blue, and green curves are the PDF curves of the X-axis

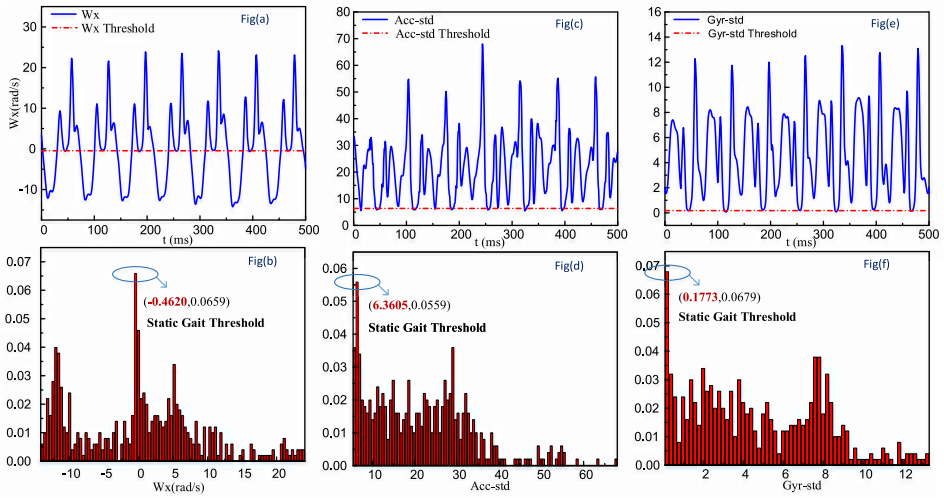

FIGURE 5. X-axis angular velocity, Standard deviation of acceleration, standard deviation of angular velocity and their probability density diagrams.

angular velocity thresholds under walking, jogging, and fast running, respectively. Points 1, 2, and 3 indicate the 90% probability that the threshold is less than the respective point value for the three-speed ranges. Among all, the threshold under walking is significantly different from those under running, while little difference exists between jogging and fast running. The standard deviation of acceleration and the standard deviation of angular velocity also have the same features. For this reason, it is possible to divide the movement patterns into walking and running.

Step 2, gait recognition. As the velocity increases, the Euclidean distance of bipedal angular velocity and acceleration increases, for which the detection equation is as follows.

$$\rho = \sqrt{{\rho_1}^T \cdot \rho_1} \qquad \rho_1 = \begin{bmatrix} f_l - f_r \\ w_l - w_r \end{bmatrix} \tag{8}$$

$$Mode = \begin{cases} 0 & \dfrac{\rho_k}{\rho_{\max}^{s\tan d}} \le 1 \\ 5 & \dfrac{\rho_k}{\rho_{\max}^{walk}} \le 1 \\ 10 & \dfrac{\rho_k}{\rho_{\max}^{walk}} > 1 \end{cases} \qquad k = 1, 2 \ldots \tag{9}$$

where f_l, f_r, w_l and w_r are the acceleration velocity and angular velocity of the left and right foot, respectively, and ρ is their Euclidean distances, $Mode$ is the motion modes, $Mode = 0$ is standing, $Mode = 5$ is walking, $Mode = 10$ is running, k is the kth moment, $\rho_{\max}^{stand}$ and $\rho_{\max}^{walk}$ are the maximum Euclidean distances in standing and walking respectively. They are calculated from the data collected in advance as shown in the following equation.

$$\begin{cases} \rho_{\max}^{s\tan d} = max(\rho_i^{s\tan d}) \\ \rho_{\max}^{walk} = max(\rho_i^{walk}) \end{cases} \qquad i \in (1, 500) \tag{10}$$

The biped data were collected for motion mode recognition by Euclidean distance, and the detection results are shown in Fig. 6. The blue curve is the Euclidean distance of biped acceleration and angular velocity, the black curve is the left foot x-axis angular velocity, and the red curve is the motion mode recognition result.

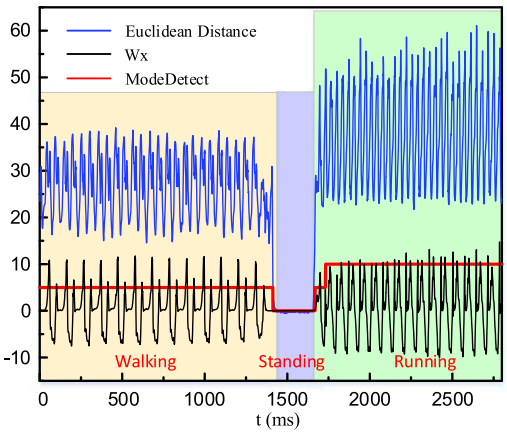

FIGURE 6. Acceleration and angular velocity Euclidean distance and motion mode recognition diagram under walking and running.

Step 3, gait detection. As shown in Fig. 7, in the still phase the foot and the ground close together, the velocity and angular velocity is approximately zero. At this time, the foot is the center of rotation, the foot-leg linkage swings forward around the O point. For that, we use the leg pitch increment and the angular velocity of the X-axis of the foot to ensure real-time zero velocity detection, while using the standard deviation of angular velocity and acceleration of the foot to ensure the reliability of the detection. And the two-node detection model is constructed as follows. When $S_1 + S_2 = 4$, it is the still phase.

$$S_1 = \begin{cases} 1 & \Delta\theta_{leg} > 0 \\ 0 & others \end{cases} \tag{11}$$

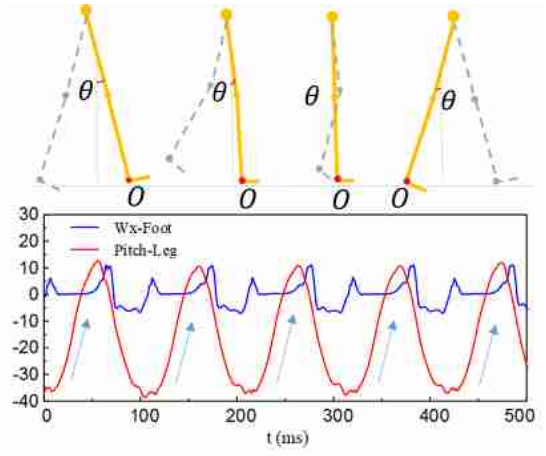

FIGURE 7. The leg movement model.

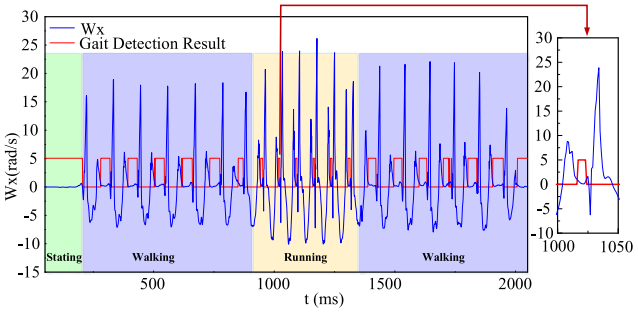

FIGURE 8. Zero-velocity detection under mixed walking and running.

$$S_2 = 3 - \min\left(\left|\frac{w_{x_k}}{Thw_x}\right|, 1\right) - \min\left(\frac{\sigma_{f_k}}{Th\sigma_f}, 1\right) - \min\left(\frac{\sigma_{w_k}}{Th\sigma_w}, 1\right) \quad (12)$$

where σ_{f_k} and σ_{w_k} represent the standard deviation of the triaxial acceleration and angular velocity at the k-th moment, w_{x_k} is the x-axis angular velocity, $\Delta\theta_{leg} = \theta_k - \theta_{k-1}$ represents the leg pitch increment, $Th\sigma_f$, $Th\sigma_w$ and Thw_x are the threshold value at the corresponding moment, respectively, S is the flag.

Collecting data under variable speed motion, the zero-velocity detection result is shown in Fig. 8, in which the blue line is the left foot x-axis angular velocity and the red line is the zero-velocity detection result. From the figure, we can be seen that the method can be adapted to different movement speeds.

D. BIPEDAL NAVIGATION SYSTEM HEADING INITIAL ALIGNMENT AND ERROR CORRECTION

It is difficult to meet the demand of navigation under vigorous motion by relying only on a single foot-mounted inertial navigation system. Therefore, we construct a biped inequality constraint to avoid a long time without error correction under vigorous motion. In the following section, the bipedal navigation system model, initial alignment, and error correction are presented.

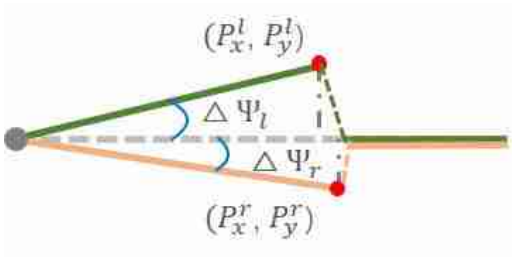

FIGURE 9. Course alignment of dual system.

(1) Course alignment of bipedal navigation system(CA)

Due to the low accuracy of IMU, it is difficult to be sensitive to the rotation of the earth for the initial alignment of the heading angle, so the heading angle is usually given as an initial value in the related papers. However, in the dual system due to the installation error, if all the initial value of heading is given the same, it will lead to the initial heading error. Current bipedal navigation systems have ignored this problem [20], [27], and even confused the initial course error with the heading angle drift error. Thus, in this paper, we propose a bipedal orientation self-alignment method, as shown in Fig. 9, assuming that the walker takes a straight line for the first three steps to constrain the heading angle.

$$\Delta\psi = a\tan(\frac{P_y}{P_x}) \quad (13)$$

$$\psi = \psi_{init} - \Delta\psi \quad (14)$$

where P_x and P_y are the positions of X-axis and Y-axis respectively, $\Delta\psi$ is the heading error angle, and ψ_{init} is the preset heading angle.

After getting the heading error angle, we correct the position of the third step. As shown in the following equation.

$$\begin{cases} P_y = P_{init\_y} \\ P_x = sqrt({P_x}^2 + {P_y}^2) \end{cases} \quad (15)$$

where P_{init_y} is the initial Y-axis position.

(2) Bipedal navigation system model

The bipedal navigation system consists of the left and right foot subsystems, which have the following states.

$$X = \begin{bmatrix} X_l & X_r \end{bmatrix} \quad (16)$$

The state vector of the left foot inertial system is $X_l = \begin{bmatrix} \delta p_l & \delta v_l & \delta\varphi_l \end{bmatrix}$, the state vector of the right foot inertial system is $X_r = \begin{bmatrix} \delta p_r & \delta v_r & \delta\varphi_r \end{bmatrix}$. $\delta p_l, \delta p_r, \delta v_l, \delta v_r, \delta\varphi_l, \delta\varphi_r$ represent the three-axis position errors, velocity errors, and attitude errors of the two subsystems, respectively.

The system state equation is as follows.

$$\dot{X} = FX + GW \quad (17)$$

where $F = \begin{bmatrix} F_l & 0_{9\times9} \\ 0_{9\times9} & F_r \end{bmatrix}$ is the system matrix for the 18 basic navigation parameters, $G = \begin{bmatrix} c_{bl}^n & c_{br}^n \end{bmatrix}$ is the error coefficient matrix, W is the Gaussian noise vector.

(3) The ZUPT

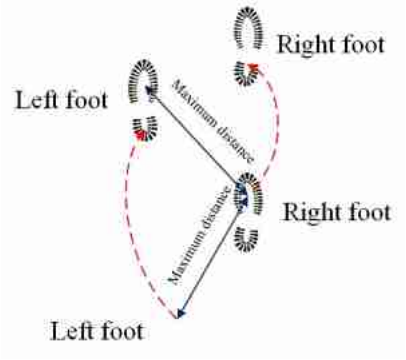

FIGURE 10. Foot movement characteristics.

ZUPT is a constraint to correct the error with zero speed when the foot touches the ground. Since the velocity is zero in the still phase, we take velocity as a observation. The measurement equations are constructed as follows.

$$Z_{zupt} = HX + V \tag{18}$$

where $Z_{zupt} = \begin{bmatrix} v_l - 0 \\ v_r - 0 \end{bmatrix}$, $H = \begin{bmatrix} 0_{3\times3} & I_{3\times3} & 0_{3\times6} & I_{3\times3} & 0_{3\times3} \end{bmatrix}$, V is the observed noise vector.

(4) Bipedal inequality constraints correction method

Reference [28] to construct the inequality constraint model. The foot motion model is shown in Fig. 10, the maximum distance between the feet during running will not exceed the maximum step length.

The constraint equation is conducted as follows.

$$\begin{cases} \tilde{X} = \max\limits_{\tilde{X}} p(\tilde{X}|Z) \\ \quad = \min\limits_{\tilde{X}} [\tilde{X}^T P^{-1} \tilde{X} - 2\hat{X}^T P^{-1} \tilde{X} + \hat{X}^T P^{-1} \hat{X}] \\ s.t. \quad \left\| L_s \tilde{X} \right\| \leq \delta\rho \end{cases} \tag{19}$$

where P is the error covariance matrix, Z is the observation vector, $\delta\rho = \rho - \rho_{\max}$, ρ is the solved bipedal distance, $\rho_{\max}$ is the maximum step length, $\hat{X}$ is the estimated state vector, L_s is the distance constraint model.

$$L_s = \begin{bmatrix} 1 & 0 & 0_{1\times7} & -1 & 0 & 0_{1\times7} \\ 0 & 1 & 0_{1\times7} & 0 & -1 & 0_{1\times7} \end{bmatrix} \tag{20}$$

If there exists a moment satisfying $\left\| L_s \tilde{X} \right\| > \delta\rho$, we consider the bipedal distance error at this time is $\delta\rho$. Linearizing $\left\| L_s \tilde{X} \right\| = \delta\rho$ and reconstructed filter constrained model as follows.

$$\kappa X^* = \tilde{\rho} \tag{21}$$

where X^* is the new state vector, $\tilde{\rho} = \delta\rho$ and $\kappa = \begin{bmatrix} 0_{1\times6} & \frac{\partial\rho}{\partial x_l} & \frac{\partial\rho}{\partial y_l} & 0 & 0_{1\times6} & \frac{\partial\rho}{\partial x_r} & \frac{\partial\rho}{\partial y_r} & 0 \end{bmatrix}$.

The updated state vector and the error covariance matrix was obtained by solving equation (19) according to [28].

$$X^* = \hat{X} - P\kappa^T (\kappa P \kappa^T)^{-1} (\kappa \hat{X} - \tilde{\rho}) \tag{22}$$

TABLE 1. Performance parameters of the inertial measurement unit.

	Angular velocity	Acceleration
Dimensions	3 axes	3 axes
Bias Stability	10 °/h	0.1mg
Full Scale	$\pm 2000°/s$	$\pm 160 m/s^2$

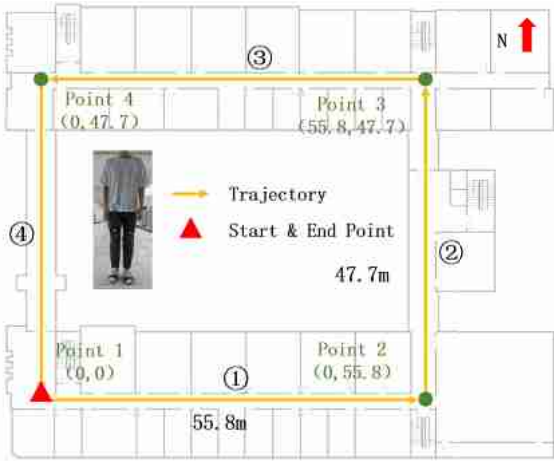

FIGURE 11. Experimental path and sensor wear diagram.

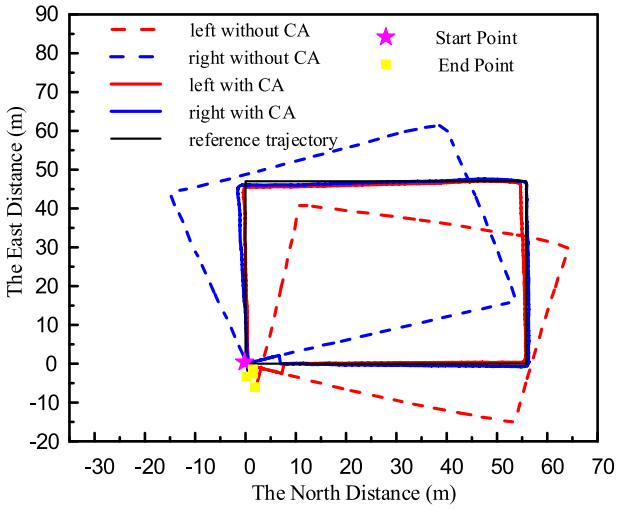

FIGURE 12. Course alignment of Bipedal navigation system.

$$P^* = (I - \mu) P (I - \mu)^T \tag{23}$$

where $\mu = P\kappa^T (\kappa P \kappa^T)^{-1} \kappa$.

E. FAULT DETECTION BY DYNAMIC KALMAN FILTER

With the increase of motion speed, the probability of zero-velocity misdetection increases which causes the observation to be abnormal. At the same time, the inequality constraint is not very accurate and the maximum step length is fixed, which will lead to false corrections. Affected by the observation error, the filter will be unstable or even divergent. Therefore, this paper detects the observation abnormality. We take the quadratic form of the observed residuals as

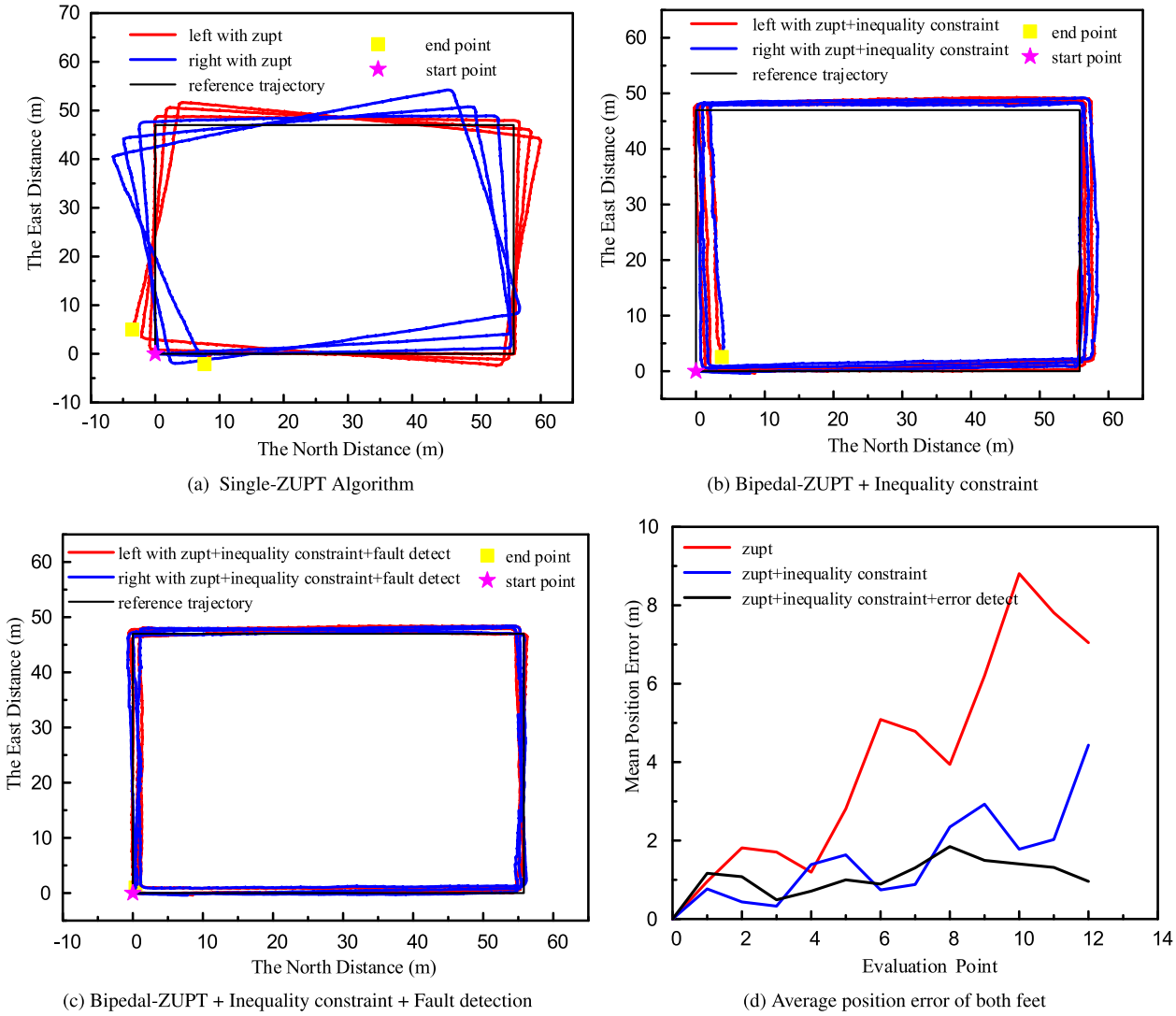

(a) Single-ZUPT Algorithm

(b) Bipedal-ZUPT + Inequality constraint

(c) Bipedal-ZUPT + Inequality constraint + Fault detection

(d) Average position error of both feet

FIGURE 13. Dual foot positioning curve of basic algorithm and improved algorithm under walking.

detection statistics.

$$T_k = V_k^T P_{k|k} V_k \tag{24}$$

where $V_k = K_k \hat{X}_k - Z_k$, K is the gain of Kalman filter, $\hat{X}$ is the state estimator, $P_{k|k}$ is the updated error covariance matrix, and Z_k is the Observation value.

Since there is 18 state, each of which is normally distributed.

$$\frac{T_k}{\sigma_0^2} \sim \chi^2(18) \tag{25}$$

where σ_0^2 is the variance factor.

Let $T_k = \frac{T_k}{\sigma_0^2}$, then when the statistics satisfy the assumptions in equation (26), it means that the observation is normal. Conversely, this step only performs state prediction without an update.

$$T_k > \chi^2(1-\alpha, 18) \tag{26}$$

where α is the confidence factor.

III. THE EXPERIMENTS AND RESULTS ANALYSIS

A. EQUIPMENT AND ENVIRONMENT

For data collection, we used the MTw Awinda inertial measurement unit. The sampling frequency of the sensor is 100Hz, the data is transmitted wirelessly. Its performance parameters are shown in Table 1. The experimental path and the sensor worn way are shown in Fig. 11, the rectangular path is 55.8m long, 47.7m wide, and 207m in total. The tester wears an IMU on both feet and both legs. The relative distances of the test route were measured by a high-precision laser rangefinder.

B. ERROR EVALUATION

To evaluate the positioning error, four reference points are set in the experimental path to calculate the error. As shown in Fig. 10, the coordinates of the reference points are (0,0), (55.8,0), (55.8,47.7), (0,47.7). As shown in equation (27), the error of each point is obtained by making the difference

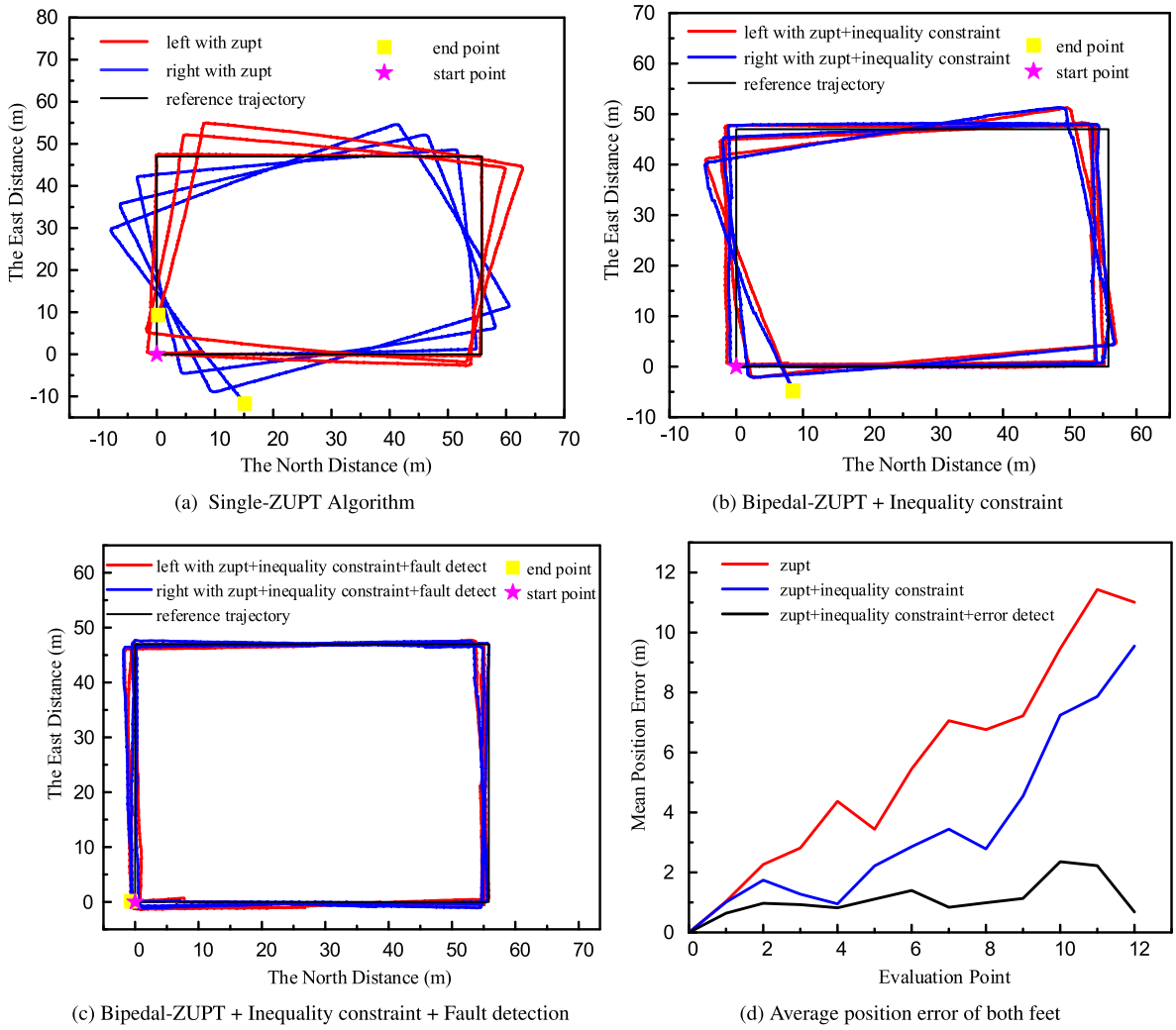

(a) Single-ZUPT Algorithm

(b) Bipedal-ZUPT + Inequality constraint

(c) Bipedal-ZUPT + Inequality constraint + Fault detection

(d) Average position error of both feet

FIGURE 14. Dual foot positioning curve of basic algorithm and improved algorithm under Running.

between the estimated position and the reference point. After obtaining the error of each point, the circular probability error(CEP) is calculated as the positioning error. The expression is as equation (28).

$$E_{i,j} = \sum_{j=1}^{k} \sum_{i=1}^{4} \left| p_m^{i,j} - p_t^{i,j} \right| \tag{27}$$

$$CEP = 1.1774 \sqrt{\frac{1}{4k} \sum_{i=1,j=1}^{4,k} E_{i,j}^2} \tag{28}$$

where $p_m^{i,j}$ is the estimated position, $p_t^{i,j}$ is the reference point, k is the repeated turns, $E_{i,j}$ position error of each point, the CEP is the final position error.

C. EXPERIMENTS

To verify the proposed bipedal system heading alignment algorithm, we conduct one comparison experiment. And to verify the adaptability of the algorithm under different movement speeds, three sets of comparison experiments were designed for slow walking, walking-running, and running movements.

1) EXPERIMENT 1: COURSE ALIGNMENT OF BIPEDAL NAVIGATION SYSTEM (CA)

In the first test, an adult male equipped with four IMUs walked at a normal speed along the experimental path. The positioning results without course alignment and with course alignment are shown in Fig. 12. The dashed line indicates the result without course alignment, and the solid line is the estimated track after course alignment, red is the left foot track and blue is the right foot track. As shown in the figure, the estimated track deviates from the actual track by the influence of the initial heading error. After getting the initial heading error angle, the following heading angles are corrected. The position error between the bipedal track and the actual track is reduced after course alignment.

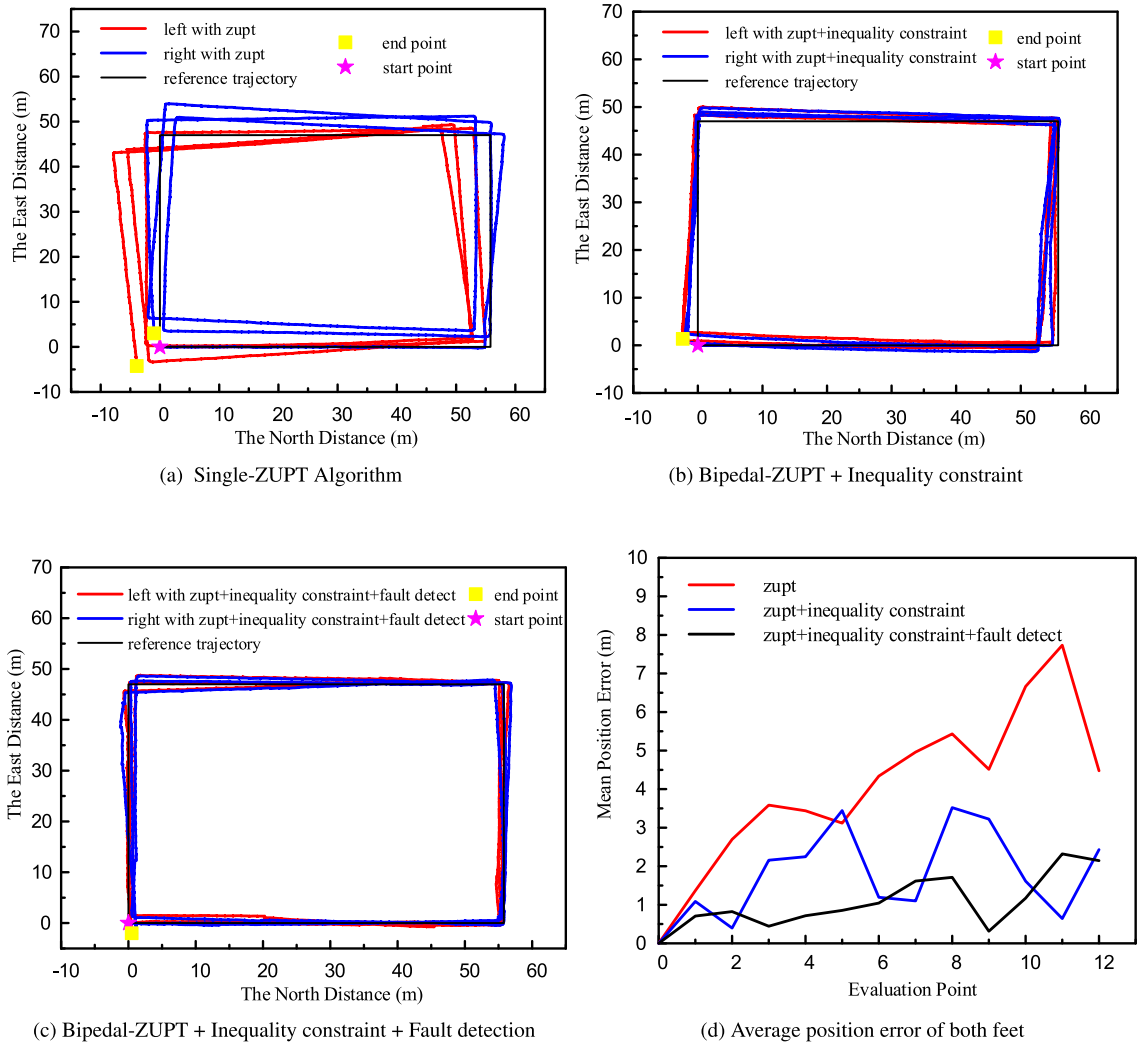

(a) Single-ZUPT Algorithm

(b) Bipedal-ZUPT + Inequality constraint

(c) Bipedal-ZUPT + Inequality constraint + Fault detection

(d) Average position error of both feet

FIGURE 15. Dual foot positioning curve of basic algorithm and improved algorithm under walking-running.

TABLE 2. Comparison of position errors for the three motion states.

Experiment	Mean position error under ZUPT(m)	Mean position error under ZUPT+ Inequality constraint(m)	Mean position error under ZUPT+ Inequality constraint+Fault detection(m)
Experiment 1 (walking)	5.73	2.24	1.35
Experiment 2 (Running)	7.75	5.32	1.46
Experiment 3 (walking-Running)	5.28	2.47	1.49

2) EXPERIMENT 2: COMPARISON OF PEDESTRIAN NAVIGATION ALGORITHMS UNDER WALKING

In the second test, an adult male equipped with four IMUs walked at a normal speed along the experimental path, and repeat 3 times. The positioning results under the bipedal-ZUPT algorithm, the bipedal-ZUPT + inequality constraint algorithm, the bipedal-ZUPT + inequality constraint + fault detection algorithm, and the average positioning error curve are shown in Fig. 13. The average positioning errors under different algorithms are shown in Table 2.

In Fig. 13(a), (b), and (c), the red curve is the track of the left foot, the blue curve is the track of the right foot, and the black curve is the reference track. The error at each evaluation point in Fig. 13(d) is the average of the left and right foot positioning errors. It can be seen from the figure that the errors accumulate over time. As seen from Table 2, the CEP errors for the three algorithms are 5.73m, 2.24m, and 1.35m, respectively. Since the algorithm proposed in this paper can achieve observations of the heading by inequality constraint, the positioning error is gradually reduced.

3) EXPERIMENT 3: COMPARISON OF PEDESTRIAN NAVIGATION ALGORITHMS UNDER RUNNING

In the third test, the same tester equipped with four IMUs ran at a speed of 6.7km/h along the experimental path, and repeat 3 times. The positioning results under the three algorithms are shown in Fig. 14.

From section II.D, it is known that the proposed fault detection method mainly detects the coarse difference of observation. Combining Fig. 14(b) and Fig. 14(c), it can be seen that in Fig. 14(b), the position are normal in the first two laps, but the heading angle error suddenly increases in the third lap, leading to the deviation from the actual trajectory in the third lap. However, in Fig. 14(c), this part of the heading angle error is eliminated, so that the navigation system can maintain the positioning accuracy. From Table 2, we can see that the CEP error under the bipetal-ZUPT algorithm is 7.75m, which is larger than the walking error. The main reason is that as the speed increases, the zero-velocity interval shortens leading to an increase in the positioning error. However, the bipedal-ZUPT + inequality constraint + fault detection algorithm proposed in this paper is equivalent to walking and running, indicating that the algorithm can be adapted to a variety of motion modes.

4) EXPERIMENT 4: COMPARISON OF PEDESTRIAN NAVIGATION ALGORITHMS UNDER WALKING-RUNNING

In the fourth test, the same tester equipped with four IMUs, moved three laps along the experimental path, including running at 7.812km/h in path 3 and walking at 4.32km/h in the rest of the path. The positioning results under the three algorithms are shown in Fig. 15.

As shown in Table 2, in the walking-running motion, the positioning errors under the three algorithms are 5.28m, 2.47m, and 1.49m, respectively. The positioning error under the bipedal-ZUPT + inequality constraint + fault detection algorithm proposed in this paper is equivalent to walking and running.

5) RESULT ANALYSIS

In Experiment 1, it is verified that the proposed course alignment method in this paper can effectively eliminate the initial heading error. In Experiment 2, the position results obtained by the bipedal-ZUPT algorithm, the bipedal-ZUPT + inequality constraint algorithm, and the bipedal-ZUPT + inequality constraint + fault detection algorithm are compared, it can be seen that the position error is decreased with the increase of the constraint. And comparing Experiments 2, 3, and 4, it can be seen that as the movement speed increases, the positioning error under ZUPT alone increases, while the bipedal-ZUPT + inequality constraint + fault detection algorithm proposed in this paper can keep the error within a certain range. The CEP errors under the three kinds of motions are 0.21%, 0.23%, and 0.23%, which are less than 0.3% of the total distance.

IV. CONCLUSION

In this paper, a four-node inertial navigation method of the human lower limb under variable speed motion has been studied. It mainly solves the four major problems under vigorous movement: low still-phase detection rate, large inertial sensors drift, difficulty in suppressing heading angle error, and the fault detection by dynamic KF. The sensor drift is estimated online by sensors' output, the model is simple and saves computation time. The thresholds of the still phase are estimated by the method of motion characteristic statistics, which can be adapted to different persons' detection. The bipedal maximum distance inequality constraint is used to correct the heading angle error. The chi-square test method is used for fault detection. Experiments show that the positioning error of the four-node inertial navigation system proposed in this paper is less than 0.3%, which can be adapted to walking, running, and variable speed motion.

The algorithm in this paper is not yet suitable for vigorous movements such as leaps and jumps. In future research, we will research the positioning method for jumping, climbing, and other vigorous movements.

REFERENCES

[1] X. Guo, N. Ansari, F. Hu, Y. Shao, N. R. Elikplim, and L. Li, "A survey on fusion-based indoor positioning," *IEEE Commun. Surveys Tuts.*, vol. 22, no. 1, pp. 566–594, 1st Quart., 2020.

[2] Y. Wu, H.-B. Zhu, Q.-X. Du, and S.-M. Tang, "A survey of the research status of pedestrian dead reckoning systems based on inertial sensors," *Int. J. Autom. Comput.*, vol. 16, no. 1, pp. 65–83, Feb. 2019.

[3] L. I. Jie and W. D. Zhang, "Research on the application of the time-serial analysis based Kalman filter in MEMS gyroscope random drift compensation," *Chin. J. Sens. Actuators*, vol. 19, no. 5, pp. 2215–2219, 2006.

[4] S. Yong, C. Jiabin, S. Chunlei, and H. Yongqiang, "Research on the compensation in MEMS gyroscope random drift based on time-series analysis and Kalman filtering," in *Proc. 34th Chin. Control Conf. (CCC)*, Jul. 2015, pp. 2078–2082.

[5] S. Zou, H. Zhang, and X. Chen, "Modeling and filter algorithm analysis of all-optical atomic spin gyroscope's random drift," in *Proc. IEEE Metrol. Aerosp. (MetroAeroSpace)*, Jun. 2015, pp. 367–371.

[6] Y. Peipei and L. Qing, "Kalman filtering of MEMS gyro based on time-series model," in *Proc. 9th Int. Conf. Electron. Meas. Instrum.*, Aug. 2009, pp. 2–367.

[7] W.-X. Qian, Q.-H. Zeng, J.-W. Wan, and Z. Xiong, "Pedestrian navigation method based on kinematic mechanism of human lower limb," *Zhongguo Guanxing Jishu Xuebao/J. Chin. Inert. Technol.*, vol. 23, no. 1, pp. 24–28, 2015.

[8] R. Harle, "A survey of indoor inertial positioning systems for pedestrians," *IEEE Commun. Surveys Tuts.*, vol. 15, no. 3, pp. 1281–1293, 3rd Quart., 2013.

[9] K. Abdulrahim, C. Hide, T. Moore, and C. Hill, "Integrating low cost IMU with building heading in indoor pedestrian navigation," *J. Global Positioning Syst.*, vol. 10, no. 1, pp. 30–38, Jun. 2011.

[10] R. Zhang, H. Yang, F. Hoflinger, and L. M. Reindl, "Adaptive zero velocity update based on velocity classification for pedestrian tracking," *IEEE Sensors J.*, vol. 17, no. 7, pp. 2137–2145, Apr. 2017.

[11] X.-L. Wang *et al.*, "Pedestrian navigation zero-speed correction method based on support vector machine classification decision," (in Chinese), *Sci. Technol. Eng.*, vol. 19, no. 1, pp. 159–165, 2019.

[12] J. Wahlstrom, I. Skog, F. Gustafsson, A. Markham, and N. Trigoni, "Zero-velocity detection—A Bayesian approach to adaptive thresholding," *IEEE Sensors Lett.*, vol. 3, no. 6, pp. 1–4, Jun. 2019.

[13] B. Wagstaff and J. Kelly, "LSTM-based zero-velocity detection for robust inertial navigation," in *Proc. Int. Conf. Indoor Positioning Indoor Navigat. (IPIN)*, Sep. 2018, pp. 1–8.

[14] I. Skog, J.-O. Nilsson, P. Handel, and A. Nehorai, "Inertial sensor arrays, maximum likelihood, and Cramér–Rao bound," *IEEE Trans. Signal Process.*, vol. 64, no. 16, pp. 4218–4227, Aug. 2016.
[15] Y. Ding, Z. Xiong, W. Li, Z. Cao, and Z. Wang, "Pedestrian navigation system with trinal-IMUs for drastic motions," *Sensors*, vol. 20, no. 19, p. 5570, Sep. 2020.
[16] J.-O. Nilsson, D. Zachariah, I. Skog, and P. Händel, "Cooperative localization by dual foot-mounted inertial sensors and inter-agent ranging," *EURASIP J. Adv. Signal Process.*, vol. 2013, no. 1, p. 164, Dec. 2013.
[17] H. Jing, J. Pinchin, C. Hill, and T. Moore, "An adaptive weighting based on modified DOP for collaborative indoor positioning," *J. Navigat.*, vol. 69, no. 2, pp. 225–245, Mar. 2016.
[18] W. Shi, Y. Wang, and Y. Wu, "Dual MIMU pedestrian navigation by inequality constraint Kalman filtering," *Sensors*, vol. 17, no. 2, p. 427, Feb. 2017.
[19] H. Zhao, Z. Wang, S. Qiu, Y. Shen, L. Zhang, K. Tang, and G. Fortino, "Heading drift reduction for foot-mounted inertial navigation system via multi-sensor fusion and dual-gait analysis," *IEEE Sensors J.*, vol. 19, no. 19, pp. 8514–8521, Oct. 2019.
[20] Q. Wang, M. Cheng, A. Noureldin, and Z. Guo, "Research on the improved method for dual foot-mounted inertial/magnetometer pedestrian positioning based on adaptive inequality constraints Kalman filter algorithm," *Measurement*, vol. 135, pp. 189–198, Mar. 2019.
[21] R. Da, "Failure detection of dynamical systems with the state chi-square test," *J. Guid., Control, Dyn.*, vol. 17, no. 2, pp. 271–277, Mar. 1994.
[22] R. Mu, S. Rong, and N. Cui, "Federated filter with strengthened FDIR capability for multiple sensor navigation system," in *Proc. 1st Int. Symp. Syst. Control Aerosp. Astronaut.*, Jan. 2006, p. 4.
[23] J. Georgy, A. Noureldin, M. J. Korenberg, and M. M. Bayoumi, "Modeling the stochastic drift of a MEMS-based gyroscope in gyro/odometer/GPS integrated navigation," *IEEE Trans. Intell. Transp. Syst.*, vol. 11, no. 4, pp. 856–872, Dec. 2010.
[24] L. F. Shi, Y. L. Zhao, G. X. Liu, S. Chen, Y. Wang, and Y. F. Shi, "A robust pedestrian dead reckoning system using low-cost magnetic and inertial sensors," *IEEE Trans. Instrum. Meas.*, vol. 68, no. 8, pp. 2996–3003, Aug. 2019.
[25] B. Wagstaff, V. Peretroukhin, and J. Kelly, "Improving foot-mounted inertial navigation through real-time motion classification," in *Proc. Int. Conf. Indoor Positioning Indoor Navigat. (IPIN)*, Sep. 2017, pp. 1–8.
[26] N. Castaneda and S. Lamy-Perbal, "An improved shoe-mounted inertial navigation system," in *Proc. Int. Conf. Indoor Positioning Indoor Navigat.*, Sep. 2010, pp. 1–6.
[27] X. Niu, Y. Li, J. Kuang, and P. Zhang, "Data fusion of dual foot-mounted IMU for pedestrian navigation," *IEEE Sensors J.*, vol. 19, no. 12, pp. 4577–4584, Jun. 2019.
[28] H. Lan, C. Yu, Y. Zhuang, Y. Li, and N. El-Sheimy, "A novel Kalman filter with state constraint approach for the integration of multiple pedestrian navigation systems," *Micromachines*, vol. 6, no. 7, pp. 926–952, Jul. 2015.

WANLING LI received the B.S. degree from the Nanjing University of Aeronautics and Astronautics, China, in 2019, where she is currently pursuing the master's degree with the Navigation Research Center. Her main research interests include indoor inertial navigation and multi-source fusion.

ZHI XIONG received the M.S. and Ph.D. degrees from the Nanjing University of Aeronautics and Astronautics (NUAA), China, in 2001 and 2004, respectively. He joined NUAA, where he has been a Full Professor with the College of Automation, since 2011. In 2013, he was an Academic Visiting Fellow with the University of Southern California, USA. He has ten years' experience in the inertial navigation field and has led more than 30 navigation system development projects. His main research interests include inertial navigation, small aircraft navigation, brain-like navigation, and multi-source fusion.

YIMING DING received the M.S. degree from Soochow University, China, in 2018. He is currently pursuing the Ph.D. degree with the Navigation Research Center, Nanjing University of Aeronautics and Astronautics, China. His main research interests include indoor inertial navigation and multi-source integration.

ZHIGUO CAO received the B.S. degree from the Nanjing University of Aeronautics and Astronautics, China, in 2019, where he is currently pursuing the master's degree with the Navigation Research Center. His main research interests include indoor inertial navigation and multi-source integration.

ZHENGCHUN WANG received the M.S. degree from the Xi'an University of Technology, China, in 2016. He is currently pursuing the Ph.D. degree with the Navigation Research Center, Nanjing University of Aeronautics and Astronautics, China. His main research interests include indoor inertial navigation and multi-source integration.